https://doi.org/10.1016/j.actamat.2019.04.041

Hardening mechanisms and impact toughening of a high-strength steel containing low Ni and Cu additions

H.J. Kong [a, 1], C. Xu [b, 1], C.C. Bu [b], C. Da [a], J.H. Luan [a, c], Z.B. Jiao [d], G. Chen [b, **], C.T. Liu [a, c,]

[a] *Department of Mechanical Engineering, City University of Hong Kong, China*

[b] *MIIT Key Laboratory of Advanced Metallic and Intermetallic Materials Technology, Engineering Research Center of Materials Behavior and Design, Ministry of Education, Nanjing University of Science and Technology, Nanjing 210094, China*

[c] *Center for Advanced Structural Materials, Department of Mechanical Engineering, City University of Hong Kong, China*

[d] *Department of Mechanical Engineering, The Hong Kong Polytechnic University, Hong Kong, China*

Abstract

Aging treatments at 400-550℃ are commonly used to attain a peak strengthening for the Cu-rich nanocluster-strengthened high-strength low-alloy (HSLA) steels. However, these temperatures fall within the dangerous 300-600℃ temper-embrittlement regime, leading to poor impact toughness. On the other hand, aging at temperatures above the embrittlement regime can improve the impact toughness but at a great expense of strength. In this work, the strengthening mechanisms as well as the toughening of a low cost weldable HSLA steel with a low content of carbon (C ~0.08 wt.%), nickel (Ni=0.78 wt.%), and copper (Cu =1.3 wt.%) were carefully investigated. Our findings show that the low-C-Ni-Cu HSLA steel is insensitive to the aging temperatures and can achieve a yield strength (YS) and ultimate tensile strength (UTS) over 1000 and 1100 MPa, respectively, with tensile ductility >10% (reduction of area >60%) at a heat-treat temperature of 640℃ through multiple strengthening mechanisms. Besides, a good low-temperature (-40℃) impact performance (~200 J) with high YS (~900 MPa) and UTS (~1000MPa) can be obtained by seeking a strength balance among the fine grain size (~2.5 mm), mediumsized (~14 nm) overaged Cu-rich precipitates, tempered martensite, and fresh martensite (or carbides). Moreover, a relatively lower YS (~800 MPa) and UTS (~900MPa)

useful for steel manufacturing can be attained by a prolonged aging at 640℃. In addition, the dislocation-precipitate interactions were also explored based on the dislocation theories in this study.

Keywords: Multiple strengthening mechanisms; Impact toughening; Temper- embrittlement; Cu-rich nanocluster-strengthened high strength; low alloy (HSLA) steel; Dislocation-precipitate interactions

1. Introduction

Cu-rich precipitation strengthening has been the limelight in high-strength low-alloy (HSLA) steel research since 1980 on replacement of the high yield (HY) steel series that are difficult to weld [1-4]. Until today, HSLA steel serves many engineering structural applications [5], from bridges, mining and dredging equipment, to critical naval and offshore applications, including the recent construction of the flight deck of the CVN-78 aircraft carriers [6], the hulls of naval ships and submarines [1,7].

Through a careful design of steel chemistry, HSLA steels with a yield strength (YS) over 1000 MPa while maintaining satisfactory ductility of 10% or more can be achieved through precipitation of a high density (approaching the order of $10^{24}/m^3$) of ultra-fine (3-5 mm) Cu-rich precipitates, as demonstrated in previous work [4,8,9]. By minute additions of 0.75 wt.% of Ni and 2 wt.% of Cu are sufficient to bring out a high number density ($7\times10^{23}/m^3$) of ultrafine (~3 nm) coherent BCC Cu precipitates. This discovery is important as it implies a significant cost reduction due to only minimal additions of Ni for a large strength improvement without sacrificing the ductility. With the advent of atom probe tomography (APT) that allows a precise probing of the chemistry and morphology of these ultra-fine metastable BCC Cu-rich precipitates, the enhanced high number density of ultra-fine Cu-rich precipitation owes mainly to the presence of a diffuse segregation of Ni at the precipitate/matrix interface. The interfacial

segregation of Ni atoms is beneficial in reducing the critical energy barrier for nucleation through the reduction of interfacial energy and the lattice misfit strain energy [8].

Despite the successful development of 1000 MPa grade ferritic HSLA steel strengthened with a high number density of ultra-fine Cu-rich precipitates through minimal Ni additions, the steel requires a peak aging at 550℃ [8] that falls within the 300-600℃ temper-embrittlement regime. The 300-600℃ temper embrittlement still remains an unsolved issue [1,10] in HSLA steels, limiting their widespread in various engineering applications, especially in turbine rotors applications. Temper embrittlement is a problem not only for the HSLA steels but for all ferritic and martensitic steels. The sinking of the Titanic and the burst of a nuclear power plant in Hinkley point in 1969 [11] are the two well-known metallurgical catastrophes due to temper embrittlement that are worth contemplating. The temper embrittlement is also known as reversible or double-step embrittlement. It is characterized by the loss of impact toughness, right shift of ductile-to-brittle transition temperature (DBTT), and brittle intergranular impact fracture along prior austenite grain boundaries. The fracture path corresponds well to the segregation of tramp elements such as phosphorus (P), antimony (Sb), tin (Sn), sulphur (S), and arsenic (As) [12] at the prior austenite grain boundaries after tempering between 300 and 600℃ or at even higher temperatures followed by slow cooling [13]. The embrittlement is even worse in the presence of Cu, Cr, Ni, and Mn [14-16]. These elements are commonly used in HSLA steels and will cosegregate with P [17], further weakening the grain boundaries by reducing their cohesion [18]. High strength contributed from the strengthened matrix in HSLA steels also encourages de-cohesion and fracture along the weakened prior austenite grain boundary [5]. In general, temper-embrittlement is not reflected in tensile properties [19]. Moreover, due to its reversibility, the temper embrittlement can be removed (de-embrittlement) by a high temperature tempering (>600℃) followed by fast quenching [13]. A short 30 s 600℃ heat treatment prior to tempering at the temper-embrittlement regime is also effective in mitigating

the temper-embrittlement as indicated by Kuzmina, Ponge, and Raabe [20]. Temper-embrittlement also causes welding problems in steels when the weldment is cooled down slowly after welding. Studies [21,22] show that a post weld treatment can alleviate the problem but at the expense of strength [22].

In this study, we aim at producing a low-C-Ni-Cu HSLA steel with a combination of high strength, satisfactory ductility, and superior low-temperature (-40℃) impact toughness by a careful control of grain size, Cu-rich precipitates, tempered martensite, and fresh martensite (or carbides) at a heat treatment temperature beyond the temper-embrittlement regime. Different from our previous work [8], in this work, while keeping the Ni level at 0.75 wt.%, the Cu content is reduced to 1.3 wt.% for reduced temper embrittlement [14] and further cost reduction. It is important to point out that our steel is insensitive to heat-treat temperatures such that the YS and UTS can be maintained at over 1000 MPa even at a heat-treat temperature of 640℃ due to multiple strengthening mechanisms. Besides, the UTS strength of our steel is insensitive to cooling rate and maintains at over 1000 MPa when it is air cooled from the 900℃ solution treatment. We have also demonstrated that, by a prolonged 10 h aging at 640℃, our steel can achieve a low YS of 800 MPa with low work hardening which is beneficial for manufacturing.

2. Experimental

Low-C-Ni-Cu HSLA steel with a nominal composition shown in Table 1 was melted with an electric-arc vacuum furnace and cast into an ingot of 55×55×55 mm. The as-cast ingot was hot rolled to 12.7mm and further cold rolled to a 10mm plate. Half of the 10mm plate was repeatedly cold rolled, solution treated at 900℃ for 30-min, and water quenched until a steel plate of 1mm final thickness with 33% of cold roll reduction for tensile test specimens. The other half 10mm plate was used for the fabrication of impact test specimens. Various heat treatment schedules were carried out on the 1mm 33% cold rolled steel plate and 10mm plate

according to Table 2.

Tensile specimens with a cross section of 3.2×1mm and a gauge length of 12.5mm were cut with electro discharge machining (EDM) such that the longitudinal side of the tensile specimens is parallel to the rolling direction. Room temperature tensile tests were performed on a MTS Alliance RT 30 tensile test machine equipped with a 10mm extensometer. The strain rate was set at 0.001/s. The yield strength was determined by the 0.2% yield off-set method.

Impact test specimens with dimensions of 55×10×10mm were EDM cut according to the GBT-229-2007 standard. A 45℃ 8mm deep V-notch was machined at the center of the specimens. The impact tests were performed with a NCS-NI500 pendulum Charpy impact tester. Prior to testing, the specimens were immersed in a low temperature tank (at a temperature 2℃ below the actual impact temperature) for more than 15-min to ensure a uniform temperature across the entire specimens. Anhydrous ethyl alcohol was used as the cooling medium. The time taken for the removal of specimens from the low temperature tank until the completion of the impact test was within 5 s.

Scanning electron microscopy (SEM) samples were prepared according to the standard mechanical grinding and polishing procedures until a final mirror-like surface finish of 0.5 mm. Etching was performed with 4 vol% of Nital solution for about 3e5 s to reveal the microscopic features for observation under a FEI Quanta FEG 450 SEM.

Transmission electron microscopy (TEM) specimens were prepared by mechanical polishing with sand papers of grit 2500 until a thickness of 50 mm, followed by punching into discs of 3mm diameter. The 3mm diameter discs were further thinned to an electron transparency with Gatan 695 precision ion polishing system before observing with a JEOL 2100 F TEM equipped with energy dispersive X-ray spectroscopy (EDX) under an operating voltage of 200 keV.

Sharp needle-shaped specimens needed for APT analysis were prepared with lift-outs and

annular milling in a FEI Scios focused ion beam/scanning electron microscope (FIB/SEM). APT was performed with a Cameca LEAP 5000 R local electrode atom probe operated in a voltage pulse-mode, with a pulse repetition rate of 200 kHz, pulse fraction of 0.2, and specimen temperature of 50 K. 3D image reconstruction and compositional analysis of Cu-rich precipitates were performed with Imago Visualization and Analysis software version 3.8.0.

As a supplement for the experimental results, thermodynamic calculations on phase fractions and elemental partitioning were performed with Thermo-Calc software version 3.1 based on TCFE 7 data base.

3. Results and discussion

3.1. Effects of heat treatments on the tensile behavior of the low-CNi-Cu HSLA steel

The production of high-strength steels with an adequate ductility, while avoiding tempering at the dangerous 300-600℃ temper-embrittlement regime, is highly desirable. The tensile properties of this steel after different heat treatments are tabulated in Table 3 and some representative stress-strain curves are selectively plotted in Fig. 1.

From Table 3, it can be seen that, after a 30-min solution treatment at 900℃ followed by water quenching (900C/WQ) alone, the steel shows an atypically high yield strength of 1017 MPa and ultimate tensile strength of 1200 MPa while keeping a satisfactory ductility of 10% (reduction of area ~63%). Nano-scale Cu-rich precipitates in the steel are expected to dissolve in the austenite solid solution, resulting in the low yield strength of this sample. This immediately suggests other strengthening mechanisms, such as martensitic transformation during 900C/WQ, must be operative in this steel. To clarify if the martensite transformation occurred on 900C/WQ, the 900℃ solutionized steel was allowed to air cool to room temperature (900C/AC). The yield strength decreases from 1017 to 870 MPa, which suggests

the possibility of reduced martensitic strengthening owing to a slower cooling rate. Even though the yield strength of the steel is reduced, it is very interesting to note that, the steel retains a high ultimate tensile strength of 1152 MPa, comparable to that of the 900C/WQ sample, together with good ductility of around 10% (reduction of area ~66%). The high work hardening of the 900C/AC sample can be ascribed to the supersaturated solid solution [23,24] and the generation of geometrically necessary dislocations due to the plastic heterogeneity of the sample during deformation [25]. The 900C/AC sample has a ferrite-bainite dual phase microstructure (section 3.3). The plastic heterogeneity arises from the strain partitioning between the soft ferrite and hard bainite. The soft ferrite will deform first and the hard bainite follows. As a result, gradients of plastic deformation are developed. To ensure compatible deformation, geometrically necessary dislocations are generated near the ferritebainite grain boundaries, contributing to the high work hardening [25-28]. In this study, grain size does not play an important role in the work hardening as all the other samples have a similar grain size of around 2.5 mm (section 3.3), yet no significant work hardening has been observed.

The 900C/WQ sample was also aged at 550℃ for 2 h, followed by air cooling (WQ/550C/2h/AC). The recorded yield strength and ultimate tensile strength are 1074 and 1159 MPa respectively, with a ductility of 13% (reduction of area ~67%). At the first thought, the yield strength of 1074 MPa seems to be comparable to that of our previous work [8] due to the peak precipitation hardening of nano-scale Cu-rich precipitates. However, at a second thought, if martensite was present, an even higher yield strength should be obtained. The yield strength (1074 MPa) of the WQ/550C/2h/AC sample seems to defy the conjecture of formation of martensite during the 900℃ water quench. In order to avoid a temper embrittlement, instead of aging at 550℃, the 900C/WQ sample was aged at 640℃ for 1 h followed by water quenching (WQ/640C/ 1h/WQ). To our surprise, the yield strength as well as the ultimate tensile strength does not change much and is still maintained at around 985 and

1038 MPa respectively, even more superior than the HSLA 115 grade steel (YS=806 MPa) used to construct the flight deck of the CVN-78 aircraft carriers. Besides, the ductility is at above 10% (reduction of area ~67%), demonstrating a great balance between high strength and ductility. More importantly, these results were obtained by avoiding the 300e600℃ embrittlement regime. Steel samples with the yield and ultimate tensile strengths of around 1000 and 1200 MPa, respectively, are attainable by adjusting the aging duration, for example, by reducing the 640℃ aging duration from 1 h to 10-min as for the WQ/640C/10min/WQ and WQ/640C/10min/AC samples.

From the application point of view, steels with a low yield strength is desirable as it can be easily cold formed during the steel processing. For this purpose, a prolonged aging at 640℃ for 10 h (WQ/640C/10h/WQ and WQ/640C/10h/AC) was performed on our steel. The yield strength and ultimate tensile strength of around 800 MPa (close to the YS of HSLA 115 grade steel) and 900 MPa, respectively, while maintaining the ductility at above 10% and the reduction of area >60%, were obtained. The work hardening is lower as compared to that of the 900C/AC sample, making these steel samples suitable for cold forming. Our steel samples exhibit an excellent necking behavior even with a yield strength over 1000 MPa and a reduction of area of >60%! This beneficial behavior can be attributed to the combined contribution from the ductile lath matensitic matrix [29,30] and the nano-scale Cu-rich precipitates (confirmed by TEM and APT studies in Section 3.3) that allow dislocations to shear through without initiating cracks [31]. In essence, it is important to indicate that our steel is insensitive to heat-treat temperatures and can attain a yield strength over 1000 MPa even after aging at 640C/10min. A steel sample with high yield (~900 MPa) and ultimate tensile strengths (~1000 MPa) while maintaining satisfactory ductility >10% and reduction of area >60% can be realized by avoiding the temper-embrittlement regime through 900C/WQ followed by a 640C/1h/WQ.

3.2. Effects of heat treatments on the impact toughness of the low-C-Ni-Cu HSLA steel

Impact resistance is an important design criterion for many engineering applications. Temper-embrittlement is one of the major causes for reduced impact toughness in ferritic and martensitic steels due to the segregation of impurities along the prior austenite grain boundaries [13,18]. To ensure the good impact toughness could be restored after the high temperature aging (640℃) beyond the temper-embrittlement regime, impact tests were carefully carried out. Impact energy serves as an indicator of the energy required for crack initiation and propagation in a test specimen [32]. Table 4 shows the impact energy of our steel under different heat treatments. It is understood that the impact and tensile specimens went through different rolling conditions. To avoid direct comparison, the tensile properties of the impact material with the same heat treatments as the impact specimens are also reported. The specimens demonstrate a low impact energy (<50 J at -20℃) when they are allowed to cool slowly (air/furnace cool) from the 900℃ solution temperature. As expected, the specimens have low impact energy after aging at temperatures within the temper-embrittlement regime. Aging at temperatures beyond the embrittlement regime (>600℃) followed by air cooling does not help to improve their impact toughness, as reflected by the low impact energy of around 20 J. On the contrary, the impact toughness of the specimens restore dramatically to more than 200 J, even at a harsher cryogenic environment of -40℃, by aging at a temperature beyond the embrittlement regime (600℃) with a subsequent water quenching. Rapid cooling, for example, water quenching after aging at a temperature above the embrittlement regime is the key to the successful impact toughness improvement. When the aging is conducted at temperatures above the 300-600℃ temper-embrittlement, potential harmful elements such as P, Cu, Cr, Ni, and Mn are boiled off from the prior austenite grain boundaries. The subsequent water quenching freezes the kinetics of embrittling elements segregating back into the prior austenite grain boundaries while the temperature passes through the 300-600℃ embrittlement regime during the cooling process.

The impact toughness of the specimens greatly improves as the grain boundary cohesion is restored. The fractography analysis (Fig. 2) reveals a brittle mixed intergranular-cleavage fracture mode for the low impact resistance (AC/600C/1h/AC) sample while a ductile dimple-like fracture mode for the high impact resistance (WQ/650C/1h/WQ) sample. The observation of intergranular fracture is in agreement with the weakening of prior austenite grain boundaries due to the 300-600℃ temper-embrittlement. As the cohesion of the prior austenite grain boundaries improves, the fracture mode changes from the brittle mixed intergranularcleavage fracture mode to the ductile dimple-like fracture. By optimizing the aging parameters such as WQ/640C/1h/WQ, our steel can achieve not only superior low-temperature (-40℃) impact toughness (~200 J), but also high yield (~900 MPa) and ultimate tensile (~1000 MPa) strengths.

3.3. Effects of heat treatments on the microstructure of the low-CNi-Cu HSLA steel

In order to understand the effects of heat treatments on the microstructure that underpins the mechanical properties of our steel samples, microstructure characterizationwas carried out with SEM and APT. The SEM images and the APT atom maps of the steel samples (1mm plate) after different heat treatments are shown in Figs. 3 and 4, respectively. Based on the SEM images, all the steel samples achieved a relatively fine grain size of approximately 2.5 mm, perhaps due to the synergistic effects of Cu and Ni additions [8]. The grain size is slightly larger than that of the Cu/Ni-steel (1.8 mm) of our previous work [8] due to a lower cold roll reduction (33%) in this study.

The SEM images (Fig. 3a and b) of the 900C/WQ sample reveal a lath martensite (M) morphology. During the 900℃ solution treatment, the steel was completely homogenized, in the form of austenitic solid solution [8]. The water quenching after the solution treatment

brought the temperature of steel down to the room temperature so rapidly that the atoms were immobilized and formed martensite. Retained austenite films [33] could be present in between the martensite laths. The remained untransformed austenitic solid solution block could also partially decompose into martensite laths and form martensite/austenite islands [34].

For the 900C/AC sample, the microstructure (Fig. 3c and d) mainly consists of bainite (B). The bainite consists of shiny needlelike grains that are encompassed within the prior austenite grain boundaries [35-37]. The shiny needle-like grains decorating the interior bainite are believed to be retained austenite or carbides or both. The retained austenite can also appear as islands at the prior austenite grain boundaries [38]. During the air cooling, polygonal ferrite (PF) formed first as it has a higher transformation temperature than the bainite [35,39]. At a high temperature, Cu precipitation in the polygonal ferrite was not favourable [39]. As the temperature went down, the solubility of C and Cu atoms reduced, resulting in a supersaturated polygonal ferrite. To relieve the supersaturation, the C and Cu atoms could either precipitate out from the supersaturated polygonal ferrite or partition to the surrounding austenite. When the temperature dropped to the bainite start temperature, bainitic transformation was initiated and the austenite transformed into bainite. Interstitial atoms such as C could precipitate out as carbides or be rejected to the surrounding austenite, stabilizing the surrounding austenite. Meanwhile, substitutional atoms such as Cu retained in the bainite during the bainitic transformation. As the temperature continued to drop, the transformation ceased. The untransformed austenite remained as retained austenite due to the enrichment of autenite stabilizers that increased the stability of the untransformed austenite against decomposition. However, depending on the stability of the retained austenite, martensite could also have formed during the final cooling to the room temperature. The APT 3D reconstructions of the 900C/AC sample (Fig. 4a) show a homogenous distribution of all atoms in the APT tip, revealing neither instances of Cu nor carbide precipitation. Thermodynamic calculations were

also performed to study the equilibrium composition of the austenite phase when our steel was air cooled from 900℃. It is understandable that, in a real situation, the equilibrium composition will not be obtained normally. Yet, it provides a quick and rough understanding of the partitioning behaviors of different elements from the polygonal ferrite to the surrounding austenite during air cooling. The thermodynamics calculations are in agreement with the partitioning of austenite stabilizers into the austenite during the air cooling, as presented in Fig. 5.

After tempering the 900C/WQ sample at 550℃ for 2 h (WQ/550C/2h/AC) and at 640℃ for 10-min (WQ/640C/10min/WQ), the martensite formed after the 900℃ water quenching decomposed into the tempered martensite, as portrayed in Fig. 3f and h. The APT 3D reconstructions of the WQ/550C/2h/AC and WQ/640C/10min/ WQ samples are presented in Fig. 4b and c, respectively. Both the samples have Cu-rich precipitates of similar size of 6.4 ± 2.8 and 7.2 ± 2.2 nm in diameter and their number density of approximately 1×10^{23} and 7.8×10^{22}/m3, respectively. The volume fraction of Cu-rich precipitates in both steel samples are estimated to be 1.37 and 1.52%, respectively. At any rate, it should be pointed out that the APT might have underestimated the actual size and overestimated the number density of the relatively large and low number density Cu-rich precipitates. The proximity histograms depicting the composition of the Cu-rich precipitates are also plotted in Fig. 6. In both the conditions, the Cu-rich precipitates are enriched with a high level of Cu (~90 at.%) at the center. Besides, the core of the Cu-rich precipitates also contain Fe (2-8 at.%), Mn (3-4 at.%), and Ni (0.6-1 at.%). A diffuse segregation of Mn (2-6 at.%) and Ni (3e7 at.%) can also be observed at the interface of the Cu precipitates. The interfacial segregation and preferential sites of elements can be related to the chemical interaction which can be explained by the heat of enthalpy mixing among the atoms [40-42]. First, Fe and Cu have a large positive mixing of enthalpy (ΔH_{mix} =13 kJ/mol [43]), suggesting a strong repulsive interaction between Fe and Cu,

leading to the origin of the nucleation of Curich precipitates. Both Mn and Ni have a repulsive interaction with Cu (ΔH_{mix} =4 kJ/mol [43]), in parallel with the segregation of Mn and Ni at the interface of Cu precipitates, most probably due to the rejection of Mn and Ni solutes from the Cu precipitates. However, Mn has a neutral interaction with Fe (ΔH_{mix} =0 [43]) while Ni has an attractive interaction with Fe (ΔH_{mix} =-2 kJ/mol [43]), resulting in Ni's preferential site towards the Fe-rich matrix and Mn's preferential site closer to the center of Cu-rich precipitates, in line with the APT results. By examining the elemental compositions far away from the Cu-rich precipitates, 79% of Cu is precipitated out from the total 1.28 wt.% of Cu for the WQ/550C/2h/AC sample while 66% of Cu diffuses out from the Fe-rich matrix into the Cu precipitates for the case of WQ/640C/10min/WQ. The balance remains in the solid solution of the Fe-rich matrix. The higher level of Cu precipitated out from the matrix of the WQ/550C/2h/AC sample than that of the WQ/640C/10min/WQ sample is in agreement with the higher Cu supersaturation that results in a higher chemical driving force for Cu precipitation due to a lower aging temperature at 550℃. One might also wonder why the Cu-rich precipitates after the 550℃ aging in the current work are larger in size (6.4 nm, ~2 times larger) and have a lower number of density (1×1023/m3, close to an order of magnitude lower) than that of our previous work [8]. This discrepancy can be due to the lower chemical driving force for nucleation in this present work due to a lower percentage of Cu (1.3 wt.%) than our previous work (2 wt.%). Another explanation for the large Cu-rich precipitates observed after the 550℃ aging in this work can be due to the rapid coarsening of Cu-rich precipitates associated with pipe and boundary diffusion encouraged by the dislocations in the martensitic matrix [44].

The microstructure of the WQ/640C/10h/WQ sample (Fig. 3j) should have extensively recovered or decomposed into ferrite and carbides [45] after the prolonged 10 h tempering at 640℃. Thermodynamic calculations were also performed to investigate the possibility of

formation of reversed austenite during the 640℃ aging. The reversed austenite could transform into a fresh martensite during the subsequent water quenching. Through the thermodynamic calculations, the onset temperature for the formation of reversed austenite (Ac1) was predicted to be at 725℃, as shown in Fig. 7. Aging at below Ac1 should not result in the formation of reversed austenite. Nevertheless, according to a study carried out by Hsiao et al. [46], it is possible to form reversed austenite after a prolonged aging below the Ac1 temperature as Curich precipitates are potential reversed austenite nucleation sites. Fresh martensite formed during the subsequent 640℃ quenching [47]. Different from the WQ/550C/2h/AC and WQ/640C/10min/WQ samples, this steel sample has large (approximately 30-50 nm in diameter) Cu-rich precipitates as shown Fig. 8a and b. The number density of the Cu-rich precipitates is approximately $5.2\times10^{20}/m^3$.

3.4. Effects of heat treatments on the strengthening mechanisms of the low-C-Ni-Cu steel

To have a clear understanding of the strengthening mechanisms of the low-C-Ni-Cu steel under different heat treatments, all strengthening components that play a part in YS were carefully examined. In this work, the strengthening arises from the combined actions of solid solution, grain size, Cu precipitates, fresh martensite, tempered martensite, bainite, and/or carbides. A base strength can be obtained from the YS of the base steel in our previous work [8]. Such base steelwas a ferritic steel with no Cu addition. An adjustment on the base strength is carried out to accommodate the slight compositional difference among the potent solution strengtheners (Mn, Mo, Si, and Cr [48,49]) that are expected to stay in the solid solution during heat treatments. This results in a base strength of 304MPa.

The strengthening due to the fine grain size can be estimated according to the Hall-Petch equation [50,51].

$$\sigma_y = \sigma_0 + k_y / \sqrt{d} \quad (1)$$

where σ_y is the yield stress, σ_0 is a material constant, k_y=600 MPa mm1/2 [52] is the Hall-Petch coefficient, and d is the grain size of the steel samples. Based on the SEM images (Fig. 3), the average grain size of the steel is approximately 2.5 mm, contributing to a strengthening of 190 MPa.

The strengthening mechanisms of nano-scale Cu-rich precipitates are still highly debatable [10,50,53]. Despite many uncertainties in the elastic modulus of the nano-scale Cu-rich precipitates [54] and the dislocation-precipitate interactions [54,55], the Russel-Brown model [56] has been quite successfully adopted in many studies [8,55]. This model was developed based on the pinning of dislocations as a result of the attractive dislocation-precipitate interaction due to the difference in the elastic modulus between the Cu-rich precipitates and the a-Fe matrix. The model operates by assuming dislocations cut through the soft Cu-rich precipitates and the resultant strengthening is described by Refs. [8,56].

$$\sigma_{Russel-Brown} = M\frac{Gb}{L}\left[1-\left(\frac{E_p}{E_m}\right)^2\right]^{\frac{3}{4}}; \sin^{-1}\left(\frac{E_p}{E_m}\right) \geq 50° \quad (2)$$

where M=3 is the Taylor factor to convert the shear stress to tensile stress, G = 80 MPa is the shear modulus of α-Fe matrix, b=0.25 nm is the Burgers vector of dislocations in the α-Fe matrix, E_p is the dislocation line energy in the Cu-rich precipitates, E_m is the dislocation line energy in the α-Fe matrix, and L is the mean spacing between the Cu-rich precipitates in the slip plane. The $\frac{E_p}{E_m}$ ratio is related to the size of the Cu-rich precipitates as follows [56].

$$\frac{E_p}{E_m} = \frac{E_p^{\infty}\log\frac{r}{r_0}}{E_m^{\infty}\log\frac{R}{r_0}} + \frac{\log\frac{R}{r}}{\log\frac{R}{r_0}} \quad (3)$$

where r is the average radius of the Cu-rich precipitates, r_0=2:5 b is the inner cut-off radius,

R=1000 r_0 is the outer cut-off radius, and $\frac{E_p}{E_m}$ =0.62 [8] is the ratio of energy per unit length of a dislocation in an infinite medium. The mean spacing between the Curich precipitates in the slip plane, L, is given by Ref. [56].

$$L = 0.866 / \sqrt{rN} \tag{4}$$

where *N* is the number density of Cu-rich precipitates. In this work, the yield strength increments predicted by the Russel-Brown model are 321, 318, and 84 MPa for the WQ/550C/2h/AC, WQ/ 640C/10min/WQ, and WQ/640C/10h/WQ samples, respectively. It is also worthwhile to make a rough estimation of the strength contribution from Cu-rich precipitation in the WQ/640C/1h/WQ sample. The size of the Cu-rich precipitates in this steel sample can be predicted according to the ($d^3 - d_0^3$) and t relation [57,58] as proposed in the Lifshitz-Slyozov-Wagner (LSW) theory [59,60].

$$d^3 - d_0^3 = kt \tag{5}$$

where *d* is the diameter of the precipitates, d_0 is the initial precipitate diameter, k is a constant, and t is the aging duration. By using the diameter of the Cu-rich precipitates of the WQ/640C/ 10min/WQ and WQ/640C/10h/WQ samples obtained from the APT and TEM analyses, the constant k and thus the size of the Cu-rich precipitates of WQ/640C/1h/WQ steel sample are calculated as 75×10^{-29} m/s and 14 nm respectively. Cu-rich precipitates of this size can contribute to a yield strength increment of approximately 200 MPa [55,61] based on the dislocation cut-through mechanism.

Apart from the Russel-Brown model that assumes the Cu-rich precipitates are soft and can be cut through by dislocations, it is also possible for the dislocations to loop around the Cu-rich precipitates as reported by Lozano-Perez et al. [54]. The strengthening due to the dislocation looping can be predicted through the Orowan looping mechanism by setting $\frac{E_p}{E_m}$ =0 [56,62] that gives

$$\sigma_{Orowon} = M\frac{Gb}{L} \quad (6)$$

The yield strength increments predicted by the Orowan looping mechanism are 1159 and 1161 MPa for the WQ/550C/2h/AC and WQ/640C/10min/WQ samples, respectively. The predicted yield strength increment by the Orowan looping mechanism far exceeds the experimental yield strength for the WQ/550C/2h/AC (experimental YS=1074 MPa) and WQ/640C/10min/WQ (1067MPa) samples, suggesting Russel-Brown model (dislocation cut-through mechanism) predicts the yield strength increment more appropriately.

The precipitation of nano-scale Cu-rich precipitates also affects the Cu and Ni contents in the solid solution of the steel matrix and thus solid solution strengthening according to the following empirical relations [49],

$$\sigma_s = 40 \times Cu\ wt.\% + 33 \times Ni\ wt.\% \quad (7)$$

where Ni wt.% and Cu wt.% are the weight percent of Ni and Cu that present in the solid solution of the steel matrix, respectively. In the 900C/WQ and 900C/AC samples, no precipitation of Cu-rich precipitates was found as discussed in Section 3.3. All Cu and Ni retained in the solid solution and resulted in a yield strength contribution of 77 MPa. For the WQ/550C/2h/AC sample, 0.27 and 0.78 wt.% of Cu and Ni dissolved in the steel matrix respectively, contributing to a yield strength increment of 37 MPa. For the WQ/ 640C/10min/WQ sample, the yield strength increment due to the respective 0.43 and 0.78 wt.% of dissolved Cu and Ni in the steel matrix is 43 MPa. For the WQ/640C/10h/WQ sample, it is assumed that all the Cu atoms were precipitated out from the solid solution to form large (~30 nm) overaged Cu-rich precipitates, leading to a yield strength contribution of 26 MPa due to the dissolved 0.78 wt.% of Ni in the steel matrix. As for the WQ/640C/1h/WQ sample, for simplicity, the solid solution strengthening is assumed to be the same as the WQ/640C/10min/WQ sample (43 MPa).

The strength contribution from fresh martensite, tempered martensite, and bainite can be

estimated by subtracting the base strength, grain size strengthening, precipitation strengthening, and the solid solution strengthening (due to Cu and Ni in the steel matrix) from the yield strength obtained from the tensile tests. To ease the visualization of the yield strength increments in the steel samples subjected to different heat treatments, a schematic diagram summarizing the strengthening components of steels is plotted in Fig. 9. A large portion of the yield strength increment (436 MPa) after 900C/WQ originates from the formation of martensite. Meanwhile, bainite contributes to a yield strength increment of 299 MPa when our steel is 900C/AC. For the WQ/550C/ 2h/AC and WQ/640C/10min/WQ samples, the yield strength increment comes from the combined action of the fine grains (~2.5 mm), slightly overaged Cu-rich precipitates (~6e8 nm) and tempered martensite. In this study, it is believed that dislocations cut through the Cu-rich precipitates instead of looping around the precipitates based on the analysis above. The fine grains (~2.5 mm), slightly overaged Cu-rich precipitates (~6-8 nm) together with the tempered martensite contribute to the yield strength increments of 773 and 720 MPa for the WQ/550C/2h/AC and WQ/640C/10min/ WQ samples respectively. For the WQ/640C/1h/WQ sample, the medium-sized overaged Cu-rich precipitates (~14 nm as predicted according to the LSW theory) contribute to a yield strength increment of 200 MPa. A strength top up from tempered martensite alone should not able to reach a yield strength increment of 248 MPa and thus it is believed that some fresh martensite (or carbides) should have also formed during the 640°C water quenching. The fine grains (~2.5 mm), medium-sized overaged Curich precipitates together with the tempered martensite and fresh martensite (or carbides) contribute to a yield strength increment of 638 MPa. In the case of the WQ/640C/10h/WQ sample, the large overaged Cu-rich precipitates (~30-50 nm) contribute to a yield strength increment of only 84 MPa by the dislocation cut-through mechanism (Fig. 10) as these precipitates are not strong enough for the dislocations to loop around [61]. The fine grains (~2.5 mm), overaged Cu-rich precipitates together with fresh martensite or carbides

contribute to a yield strength increment of 541 MPa.

4. Summary

Based on the systematic study on the effects of heat treatments on the tensile properties, microstructure, strengthening mechanism, and the impact performances of the low-C-Ni-Cu HSLA steel, the following conclusions can be drawn:

1) Gigapascal-grade steel sample with the YS and UTS over 1000 MPa, the ductility more than 10%, and the reduction of area >60% can be obtained by water quenching after a 900℃ solution treatment followed by a short 10-min aging at 640℃. A yield strength increment of 720 MPa is achieved through a combined strengthening from the fine grain size (~2.5 mm), slightly overaged Cu-rich rich precipitates (~6-8 nm) and tempered martensite. The realization of the GPa-grade HSLA steel without the temper-embrittlement at 300-600℃ is possible through multiple strengthening mechanisms.

2) High-strength steel sample with YS ~900 MPa, UTS ~1000 MPa, ductility >10%, and reduction of area >60%, together with a superior low-temperature impact toughness (~200 J at -40℃) can be obtained by an optimized heat treatment condition, for instance, WQ/640C/1h/WQ. A yield strength increment of 638 MPa is achieved through a combined action of fine grain size (~2.5 mm), medium-sized overaged Cu-rich precipitates (~14 nm), tempered martensite and fresh martensite (or carbides) during the 640℃/WQ.

3) A steel sample with a relatively lower YS (~870 MPa) while keeping the UTS at over 1000 MPa can be obtained by the 900℃/AC solution treatment. The low YS is attributed to the formation of bainite during air cooling. Meanwhile, the high work hardening of the steel is due to the supersaturated solid solution and the generation of geometrically necessary dislocations in the ferrite-bainite dual phase steel during deformation.

4) Low-strength steel sample with YS ~800 MPa, UTS ~900 MPa, and low work

hardening can be obtained by a prolonged aging at 640℃ for 10 h after the 900 □C solution treatment. A yield strength increment of 541 MPa is obtained through the fine grain size (~2.5 mm), large overaged Cu-rich precipitates (~30-50 nm) and the formation of fresh martensite (or carbides) during the 640℃ water quenching. This steel sample is important for applications where a large amount of cold fabrication and forming is required for production.

5) The steel exhibits a good necking behavior and large area reduction even for steel samples with strength over 1000 MPa. A large deformation can be sustained during cold work and forming. This beneficial property can be attributed to the ductile lath martensite matrix and nano-scale Cu-rich precipitates that allow dislocations to cut through easily without initiating cracks. Dislocation shearing mechanism is believed to be operative for Cu-rich precipitates ranging from 5 to 50 nm.

Acknowledgement

This research was supported by the Research Grant Council of the Hong Kong Special Administrative Region, China (CityU 11205515) and National Natural Science Foundation of China (grant number 51571117).

References

[1] S.K. Dhua, A. Ray, D.S. Sarma, Effect of tempering temperatures on the mechanical properties and microstructures of HSLA-100 type copper-bearing steels, Mater. Sci. Eng. 318 (2001) 197-210.

[2] D. Jain, D. Isheim, A.H. Hunter, D.N. Seidman, Multicomponent high-strength low-alloy steel precipitation-strengthened by sub-nanometric Cu precipitates and M2C carbides, Metall. Mater. Trans. 47 (A) (2016) 3860-3872.

[3] B.A. Graville, Cold cracking in wleds in HSLA steels, in: Welding of HSLA (Micro alloyed) Structural Steels- Proceedings of an International Conference, Ohio, USA, 1978.

[4] M.E. Fine, S. Vaynman, D. Isheim, Y.W. Chung, S.P. Bhat, C.H. Hahin, A new paradigm for

designing high-fracture-energy steels, Metall. Mater. Trans. 41 (13) (2010) 3318-3325.

[5] S.K. Dhua, D. Mukerjee, D.S. Sarma, Influence of tempering on the microstructure and mechanical properties of HSLA-100 steel plates, Metall. Mater. Trans. 32A (2001) 2259-2270.

[6] National Research Council, Division on Engineering and Physical Sciences, National Materials and Manufacturing Board, Committee on Benchmarking the Technology and Application of Light weighting, Application of Light weighting Technology to Military Aircraft, Vessels, and Vehicles, National Academies Press, Washington, DC, 2012.

[7] E.J. Czyryca, Advances in high strength steel technology for naval hull construction, Key Eng. Mater. 84-85 (1993) 495-520.

[8] Z.B. Jiao, J.H. Luan, Z.W. Zhang, M.K. Miller, W.B. Ma, C.T. Liu, Synergistic effects of Cu and Ni on nanoscale precipitation and mechanical properties of high-strength steels, Acta Mater. 61 (2013) 5996-6005.

[9] S. Vaynman, D. Isheim, R.P. Kolli, S.P. Bhat, D.N. Seidman, M.E. Fine, Highstrength low-carbon ferritic steel containing Cu-Fe-Ni-Al Mn precipitates, Metall. Mater. Trans. 39 (2) (2008) 363-373.

[10] H.J. Kong, C.T. Liu, A review on nano-scale precipitation in steels, Technologies 6 (1) (2018) 36.

[11] D. Kalderon, Steam turbine failure at Hinkley point 'A', Proc. Inst. Mech. Eng. 186 (1) (1972) 341-377.

[12] J.B. Rellick, C.J. McMahon, Intergranular embrittlement of iron-carbon alloys by impurities, Metall. Trans. 5 (11) (1974) 2439-2450.

[13] C.J. McMahon Jr., J.R. Rellick, B. Schulz, Intergranular Embrittlement in Ferrous Alloys, ICF2, Brighton (UK), 1969.

[14] M. Hasegawa, N. Nakajima, N. Kusunoki, K. Suzuki, Effects of copper and phosphorus on temper embrittlement of Mn-Mo-Ni low alloy steel (ASTM A533-B), Trans. Jpn. Inst. Met. 16 (10) (1975) 641-646.

[15] S. Park, K. Lee, K. Min, M. Kim, B. Lee, Influence of the thermodynamic parameters on the temper embrittlement of SA508 Gr.4N Ni-Cr-Mo low alloy steel with variation of Ni, Cr and Mn contents, J. Nucl. Mater. 426 (2012) 1-8.

[16] D. Isheim, R.P. Kolli, M.E. Fine, D.N. Seidman, An atom-probe tomographic study of the temporal evolution of the nanostructure of Fe-Cu based highstrength low-carbon steels, Scripta Mater. 55 (2006) 35-40.

[17] M. Guttmann, The role of residuals and alloying elements in temper embrittlement, Phil.

Trans. Roy. Soc. Lond. 295 (1980) 169-196.

[18] E.D. Hondros, M.P. Seah, S. Hofmann, P. Lejcek, Interfacial and surface microchemistry, in: The Netherland, Physical Metallurgy, vol. 2, North- Holland, 1996, pp. 1202-1289.

[19] R. Viswanathan, Damage Mechanisms and Life Assessment of High Temperature Components, ASM International, USA, 1989.

[20] M. Kuzmina, D. Ponge, D. Raabe, Grain boundary segregation engineering and austenite reversion turn embrittlement into toughness: example of a 9 wt.% medium Mn steel, Acta Mater. 86 (2015) 182-192.

[21] J. Grosse-Wordemann, S. Dittrich, Prevention of Temper Embrittlement in 2.25 Cr- 1 Mo Weld Metal by Metallurgical Actions, Welding Research Supplement, 1983, pp. 123-128.

[22] Z.B. Jiao, J.H. Luan, W. Guo, J.D. Poplawsky, C.T. Liu, Effects of welding and post -weld heat treatments on nanoscale precipitation and mechanical properties of an ultra-high strength steel hardened by NiAl and Cu nanoparticels, Acta Mater. 120 (2016) 216-227.

[23] J. d. Costa Teixeira, Y. Brechet, Y. Estrin, C. Hutchinson, The strain hardening behaviour of supersaturated Al-Cu alloys, in: Proceedings of the 12th International Conference on Aluminium Alloys, Japan, Yokohama, Sept 5-9, 2010.

[24] A. Deschamps, S. Esmaeili, W.J. Poole, M. Militzer, Strain hardening rate in relation to microstructure in precipitation hardening materials, J. Phys. IV France 10 (2000) Pr6, 151-156.

[25] M.M. Karimi, S. Kheirandish, Comparison of work hardening behaviour of ferritic-bainitic and ferritic-martensitic dual phase steels, Steel Res. Int. 80 (2) (2009) 160-164.

[26] M.F. Ashby, The deformation of plastically non-homogeneous materials, Phil. Mag. 21 (170) (1970) 399-424.

[27] X. Wu, Y. Zhu, Heterogeneous materials: a new class of materials with unprecedented mechanical properties, Mater. Res. Lett. 5 (8) (2017) 527-532.

[28] M. Calcagnotto, Y. Adachi, D. Ponge, D. Raabe, Deformation and fracture mechanisms in fine- and ultrafine-grained ferrite/martensite dual-phase steels and the effect of aging, Acta Mater. 59 (2) (2011) 658-670.

[29] S.W. Thompson, Microstructural characterization of an as-quenched HSLA- 100 plate steel via transmission electron microscopy, Mater. Char. 77 (2013) 89-98.

[30] A.S. Schulz-Beenken, Martensite in steels: its significance, recent developments and trends, J. Phys. IV France 7 (C5) (1997) 359-366.

[31] S. Jiang, H. Wang, Y. Wu, X. Liu, H. Chen, M. Yao, B. Gault, D. Ponge, D. Raabe, A.

Hirata, M. Chen, Y. Wang, Z. Lu, Ultra strong steel via minimal lattice misfit and high-density nanoprecipitation, Nature 0 (2017) 1-5.

[32] L. Lan, C. Qiu, D. Zhao, X. Gao, L. Du, Microstructural characteristics and toughness of the simulated coarse grained heat affected zone of high strength low carbon bainitic steel, Mater. Sci. Eng. 529 (2011) 192-200.

[33] A. Navarro-Lopez, J. Hidalgo, J. Sietsma, M.J. Santofimia, Characterization of bainitic/martensitic structures formed in isothermal treatments below the Ms temperature, Mater. Char. 128 (2017) 248-256.

[34] H.L. Yi, P. Chen, H.K.D.H. Bhadeshia, Optimizing the morphology and stability of retained austenite in a d-TRIP steel, Metall. Mater. Trans. 45 (A) (2014) 3512-3518.

[35] Q.D. Liu, S.J. Zhao, Comparative study on austenite decomposition and Cu precipitation during continuous cooling transformation, Metall. Mater. Trans. 44 (1) (2013) 163-171.

[36] A.P. Coldren, J.L. Mihelich, Acicular ferrite HSLA steels for line pipe, Met. Sci. Heat Treat. 19 (7) (1977) 559-572.

[37] H.K.D.H. Bhadeshia, Bainite in Steels, Maney Publishing, UK, 2015.

[38] Z. Yang, Z. Liu, X. He, S. Qiao, C. Xie, Effect of microstructure on the impact toughness and temper embrittlement of SA508Gr. 4N steel for advanced pressure vessel materials, Sci. Rep. 8 (207) (2018) 1-12.

[39] Q. Liu, W. Liu, Correlation of Cu precipitation with austenite-ferrite transformation in a continuously cooled multicomponent steel: an atom probe tomography study, J. Mater. Res. 27 (7) (2012) 1060-1067.

[40] Z.B. Jiao, J.H. Luan, M.K. Miller, C.Y. Yu, C.T. Liu, Effects of Mn partitioning on nanoscale precipitation and mechanical properties of ferritic steels strengthened by NiAl nanoparticles, Acta Mater. 84 (2015) 283-291.

[41] W. Hume-Rothery, E. Anderson, Eutectic compositions and liquid immiscibility in certain binary alloys, Phil. Mag. 5 (52) (1960) 383-405.

[42] D. Isheim, M.S. Gagliano, M.E. Fine, D.N. Seidman, Interfacial segregation at Cu-rich precipitates in a high-strength low-carbon steel studied on a sub nanometer scale, Acta Mater. 54 (3) (2006) 841-849.

[43] A. Takeuchi, A. Inoue, Classification of bulk metallic glasses by atomic size difference, heat of mixing and period of constituent elements and its application to characterization of the main alloying element, Mater. Trans. 46 (12) (2005) 2817-2829.

[44] N. Maruyama, M. Sugiyama, T. Hara, H. Tamehiro, Precipitation and phase transformation of copper particles in low alloy ferritic and martensitic steels, Mater. Trans.

40 (4) (1999) 268-277.

[45] R. Varughese, P.R. Howell, The application of transmission electron microscope to the study of a low-carbon steel: HSLA-100, in: Metallogrphy: Past, Present, and Future, ASTM, Philadelphia, USA, 1993, pp. 199-211.

[46] C.N. Hsiao, C.S. Chiou, J.R. Yang, Aging reactions in a 17-4 PH stainless steel, Mater. Chem. Phys. 74 (2002) 134-142.

[47] M. Mujahid, A.K. Lis, C.I. Garcia, A.J. De Ardo, HSLA-100 steels: influence of aging heat treatment on microstructure and properties, J. Mater. Eng. Perform. 7 (1998) 247-257.

[48] W.C. Leslie, Iron and its dilute substitutional solid solutions, Metall. Trans. 3 (1972) 5-26.

[49] F.B. Pickering, Physical Metallurgy and Design of Steels, Applied Science Publisher, London, 1978.

[50] E.O. Hall, The deformation and aging of mild steel: III discussion of results, Proc. Phys. Soc. B 64 (9) (1951) 747-753.

[51] N.J. Petch, The cleavage strength of polycrystals, J. Iron Steel Inst. 174 (1953) 25-28.

[52] S. Takaki, K. Kawasaki, Y. Kimura, Mechanical properties of ultra fine grained steels, J. Mater. Process. Technol. 117 (2001) 359-363.

[53] M.E. Fine, D. Isheim, Origin of copper precipitation strengthening in steel revisited, Sripta Mater. 53 (1) (2005) 115-118.

[54] S. Lozano-Perez, M.L. Jenkins, J.M. Titchmarsh, Evidence for deformation induced transformations of Cu-rich precipitates in an aged FeCu alloy, Phil. Mag. Lett. 86 (6) (2006) 367-374.

[55] J. Takahashi, K. Kawakami, Y. Kobayashi, Consideration of particle strengthening mechanism of copper-precipitation-strengthened steels by atom probe tomography analysis, Mater. Sci. Eng. 535 (2012) 144-152.

[56] K.C. Russel, L.M. Brown, A dispersion strengthening model based on differing elastic moduli applied to the iron-copper system, Acta Metall. 20 (7) (1972) 969-974.

[57] R. Monzen, K. Takada, K. Matsuda, Coarsening kinetics of Cu particles in an Fe- 1.5 % Cu alloy, Z. Met. 94 (11) (2003) 1241-1246.

[58] R. Monzen, K. Takada, W. Chihiro, Coarsening of spherical Cu particles in an a- Fe matrix, ISIJ Int. 44 (2) (2004) 442-444.

[59] C. Wagner, Theorie der alterung von niederschlägen durch umlösen (Ostwald- Reifung), Z. für Elektrochem. 65 (7-8) (1961) 581-591.

[60] I.M. Lifshitz, V.V. Slyozov, The kinetics of precipitation from supersaturated solid

solutions, J. Phys. Chem. Solids 19 (1-2) (1961) 35-50.

[61] K. Nakashima, Y. Futamura, T. Tsuchiyama, S. Takaki, Interaction between dislocation and copper particles in Fe-Cu alloys, ISIJ Int. 42 (12) (2002) 1541-1545.

[62] J.W. Martin, Precipitation Hardening, Butterworth-Heinemann, Oxford, UK, 1998.

Table 1 The elemental composition (wt.%) of the low-C-Ni-Cu HSLA steel.

C	Ni	Cu	Mn	V	Cr	Ti	Mo	Fe
0.07	0.78	1.28	0.53	0.20	2.41	0.05	0.80	balance

Table 2 The heat treatment schedules of the low-C-Ni-Cu HSLA steel.

Steel	Heat treatment
900C/WQ	900℃30-min WQ
900C/AC	900℃30-min AC
900C/FC	900℃30-min FC
WQ/450C/1h/AC	900℃30-min AC+450℃1hAC
WQ/550C/2h/AC	900℃30-min WQ+550℃2hAC
WQ/600C/1 h/WQ	900℃30-min WQ+600℃1hWQ
WQ/640C/10min/WQ	900℃30-min WQ+640℃10-minWQ
WQ/640C/10min/AC	900℃30-min WQ+640℃10-minAC
WQ/640C/1 h/WQ	900℃30-min WQ+640℃1hWQ
WQ/640C/10h/WQ	900℃30-min WQ+640℃10hWQ
WQ/640C/10h/AC	900℃30-min WQ+640℃10hAC
WQ/650C/1 h/WQ	900℃30-min WQ+650℃1hWQ
AC/580C/1h/AC	900℃30-min AC+580℃1hAC
AC/600C/1h/AC	900℃30-min AC+600℃1hAC
AC/620C/1h/AC	900℃30-min AC+620℃1hAC
WQ: water quenched AC: air cooled FC: furnace cooled	

Table 3 The tensile performances of the low-C-Ni-Cu HSLA steel with difference heat treatments. YS: yield strength; UTS: ultimate tensile strength; % El: tensile elongation; RA: reduction of area.

	YS(MPa)	UTS(MPa)		%El	RA(%)
900C/WQ	1017±14	1200±13		10±1	63
900C/AC	870±10	1152±7		10±1	66
WQ/550C/2h/AC	1074±11	1159±15		13±1	67
WQ/640C/10min/WQ	1067	1124		11	68
WQ/640C/10min/AC	1138	1201		13	66
WQ/640C/1h/WQ	985	1038		12	67
WQ/640C/10h/WQ	871	938		11	69
WQ/640C/10h/AC	817	889		13	70

Table 4 The impact energy along with the room temperature tensile properties of the low-CNi-Cu steel after different heat treatments. AC: air cool; FC: furnace cool; WQ: water quench; OQ: oil quench; YS: yield strength; UTS: ultimate tensile strength.

	Impact Energy (J)		
Tested at -20℃			
900C/AC	37 ± 4		
900C/FC	43 ± 6		
AC/620C/1h/AC	23 ± 15		
AC/600C/1hAC	19 ± 1		
AC/580C/1h/AC	18 ± 5		
WQ/450C/1h/AC	4±2	1177±21	1238±12
Tested at -40℃			
WQ/650C/1h/WQ	208±36	925±4	976±2
WQ/600C/1h/WQ	152±20	1070±6	1118±9

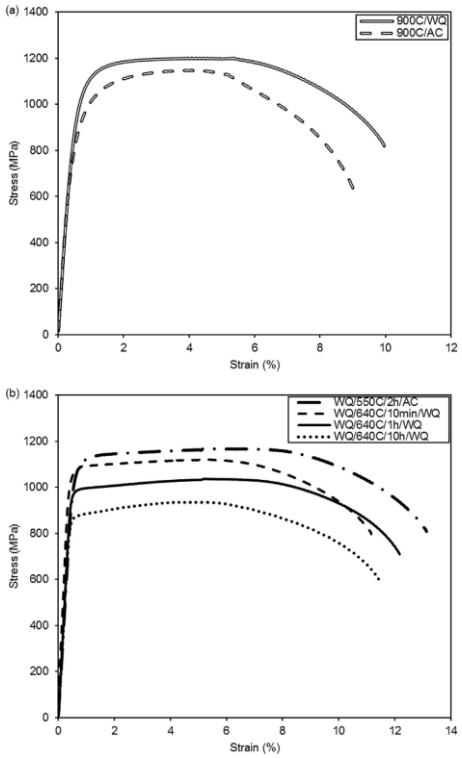

Fig. 1. Selective room temperature stress-strain curves of (a) 900C/WQ and 900C/AC samples and (b) WQ/550/2h/AC, WQ/640C/10min/WQ, WQ/640C/1h/WQ, and WQ/640C/10h/WQ samples.

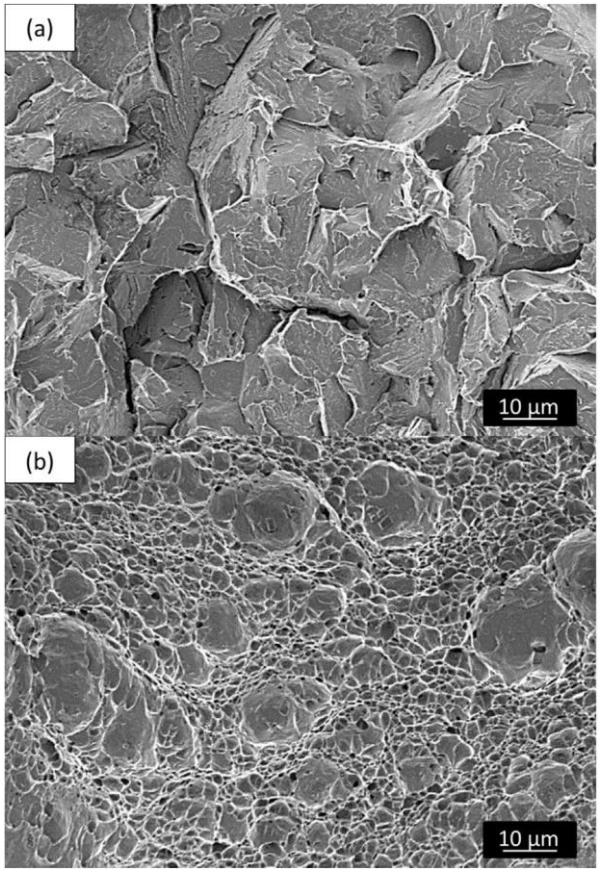

Fig. 2. Fracture surfaces of (a) AC/600C/1h/AC and (b) WQ/650C/1h/WQ samples after impact test.

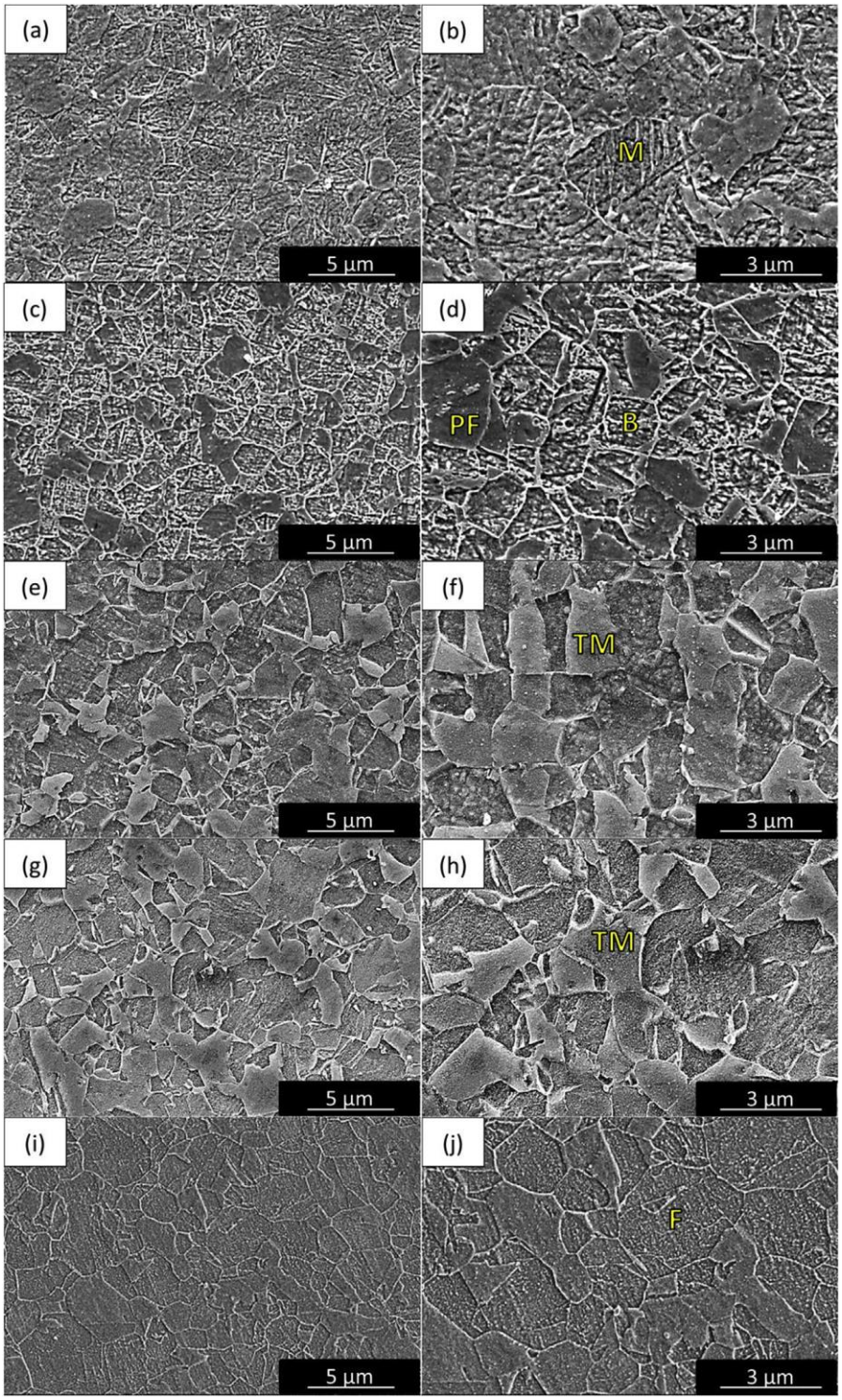

Fig. 3. SEM images of (a); (b) 900C/WQ, (c); (d) 900C/AC, (e); (f) WQ/550C/2h/AC, (g); (h) WQ/640C/10min/WQ, and (i); (j) WQ/640C/10h/WQ samples. M: martensite; PF: polygonal ferrite; B: bainite; TM: tempered martensite; F: ferrite.

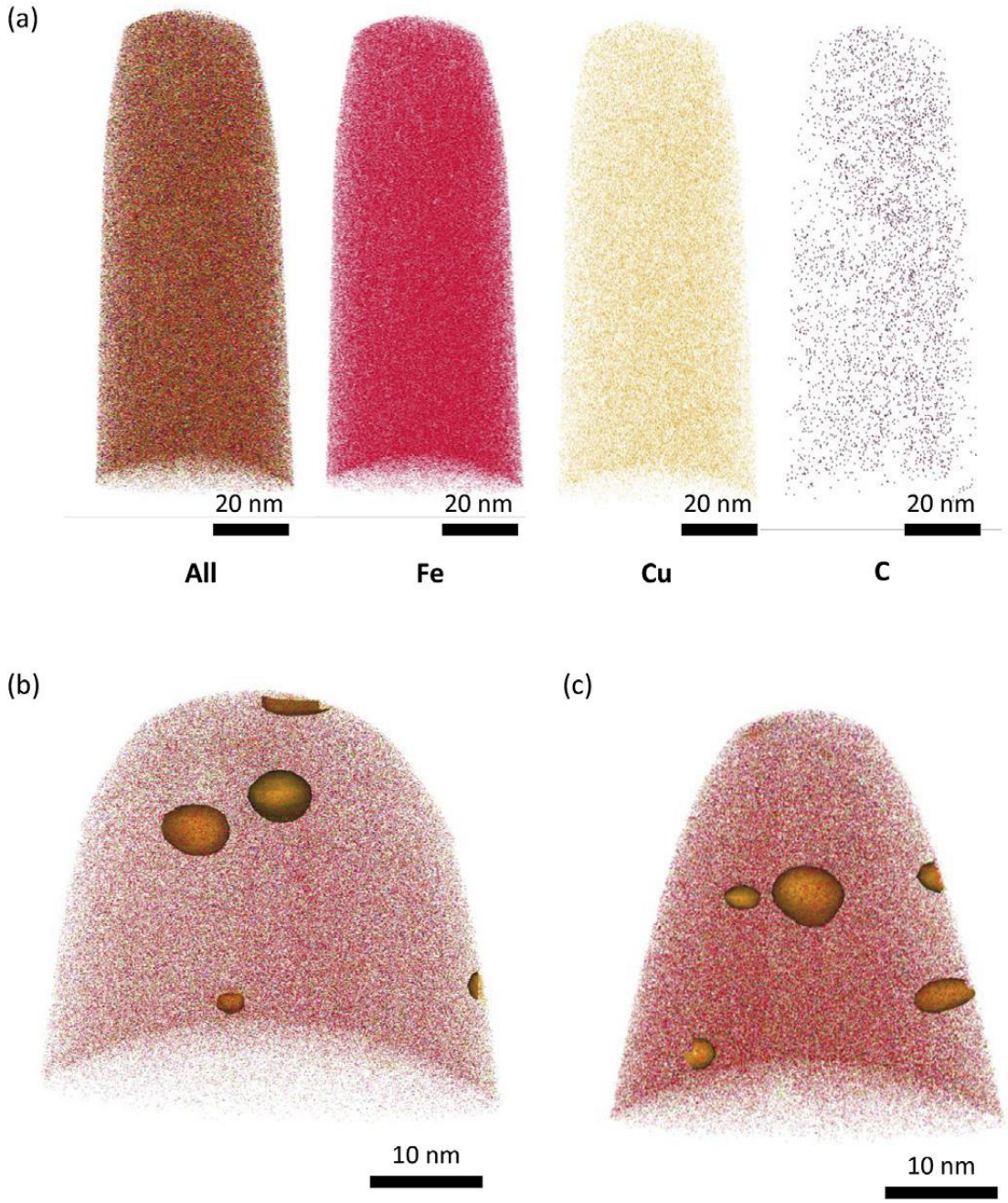

Fig. 4. APT 3D reconstructions showing the atom maps of (a) 900C/AC sample, (b) WQ/ 640C/10min/WQ sample, and (c) WQ/550C/2h/AC sample at 10 at.% Cu isoconcentration surfaces.

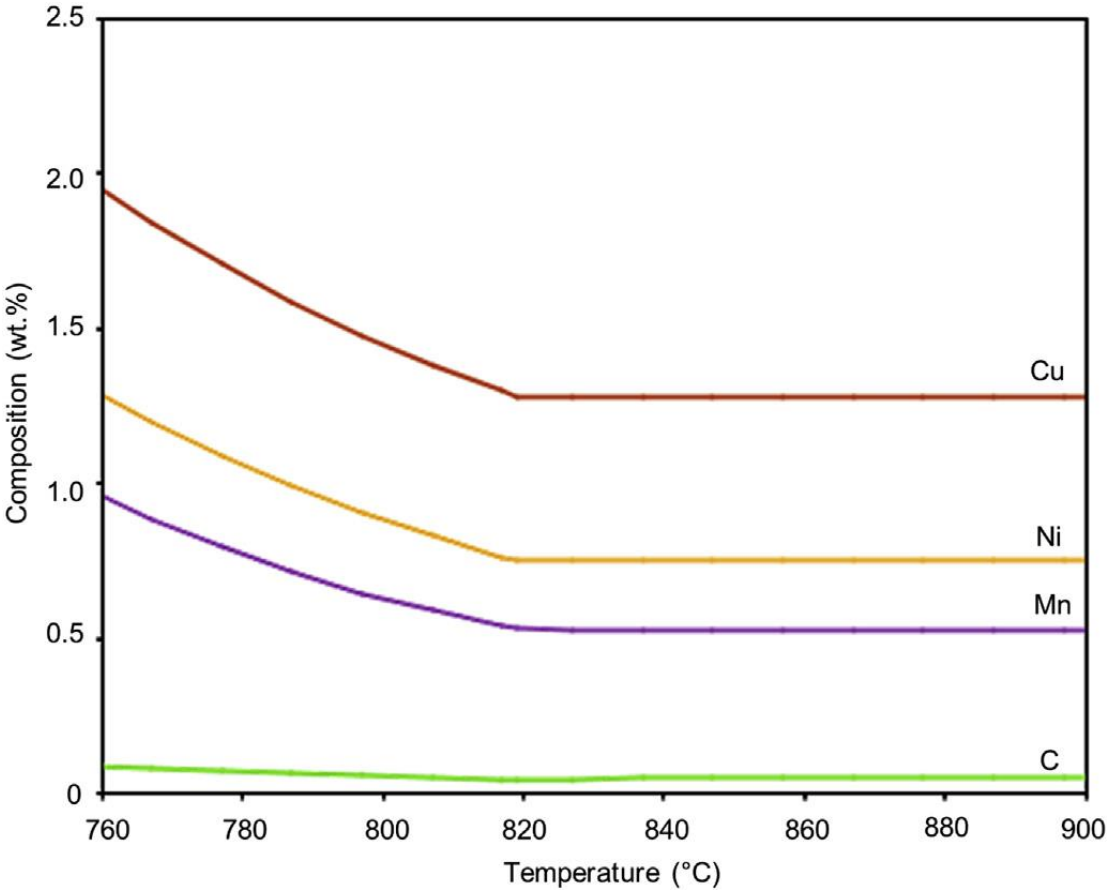

Fig. 5. Thermodynamics calculation showing the elemental composition of the austenite phase as a function of temperature.

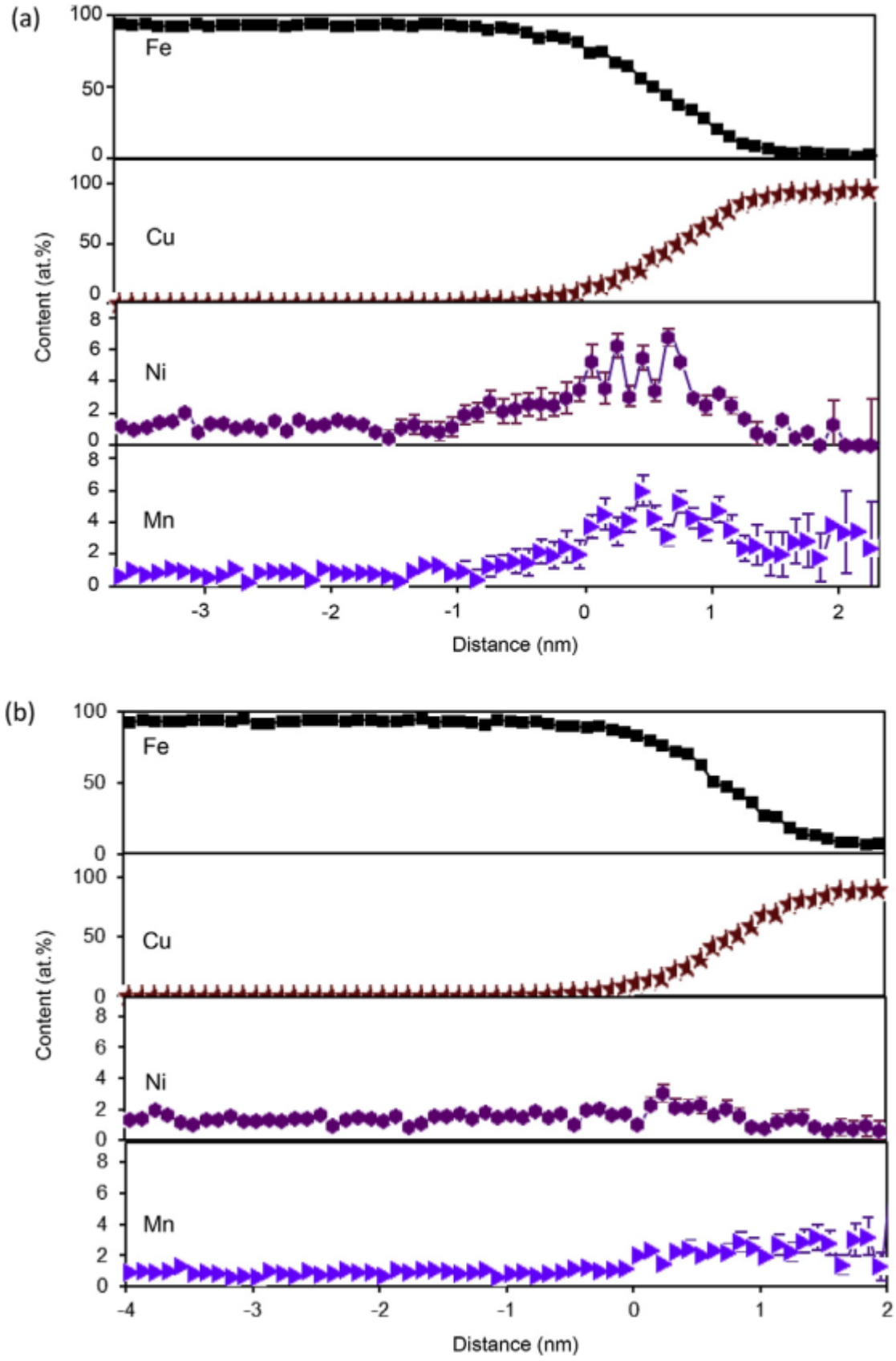

Fig. 6. Proximity histograms of Cu precipitates for (a) WQ/550C/2h/AC and (b) WQ/640C/10min/WQ samples.

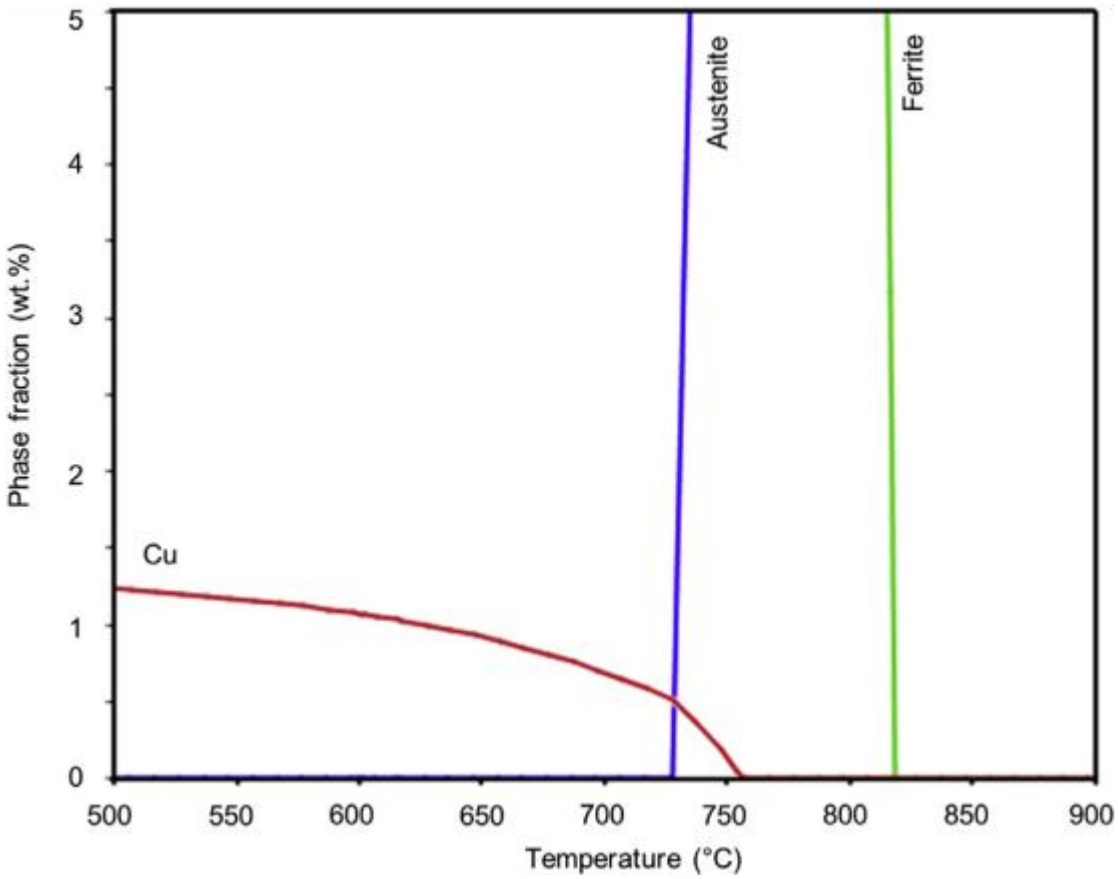

Fig. 7. Thermodynamic calculation showing the phase fraction as a function of temperature.

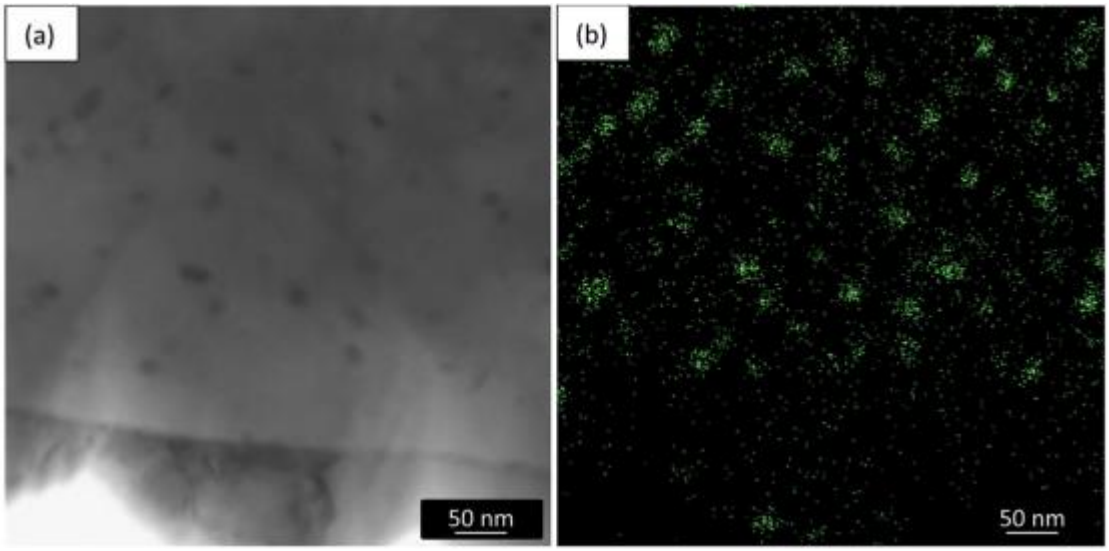

Fig. 8. STEM images of WQ/640C/10h/WQ sample showing the presence of (a) overaged Cu-rich precipitates and (b) EDX elemental mapping of the Cu-rich precipitates. The size and the number density of the Cu-rich precipitates are approximated to be around 30-50 nm and $5.2\times10^{20}/m^3$, respectively.

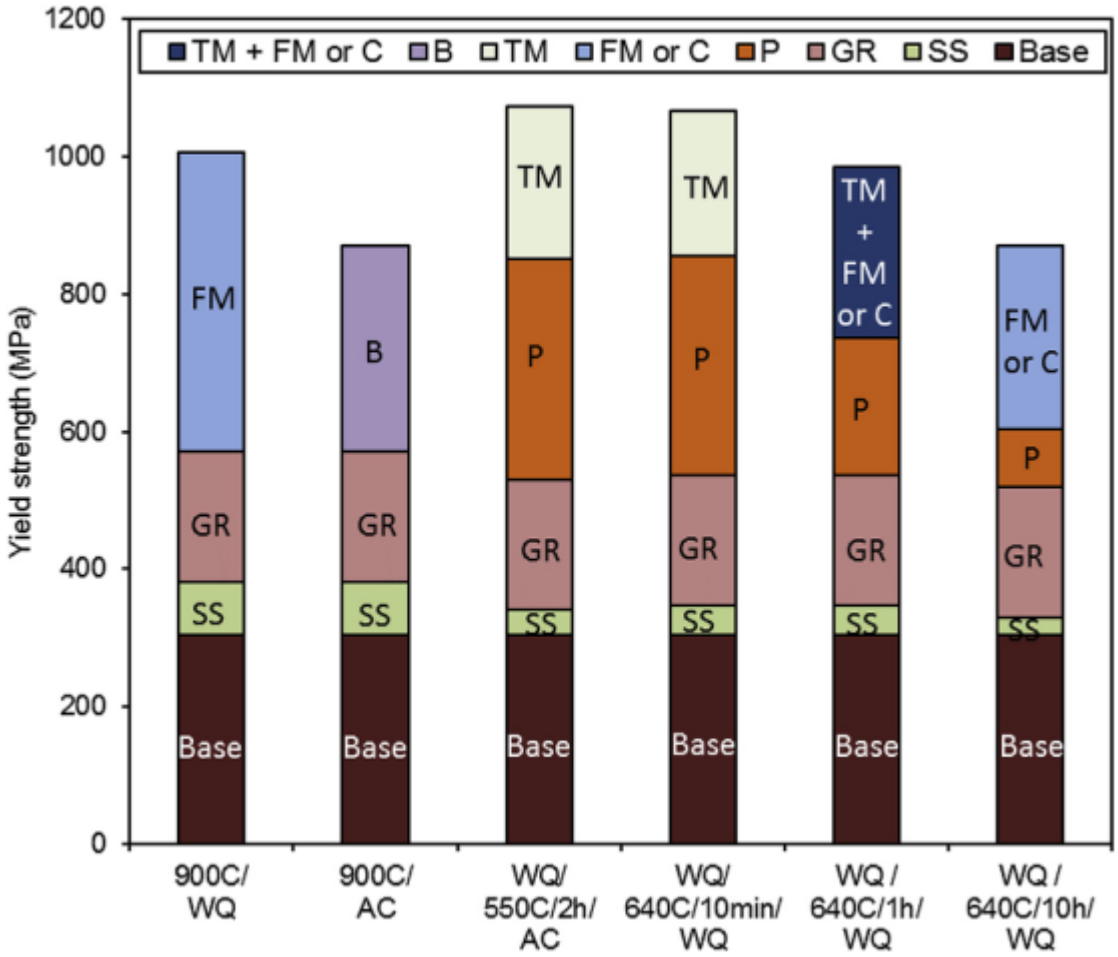

Fig. 9. The strengthening mix of the low-C-Ni-Cu steel after different heat treatments. Adjustment was made to accommodate the difference in base strength due to potent solid solution strengtheners (Mn, Mo, Si, and Cr) between the steels in this study and our previous work [8]. B: bainite strengthening; TM: tempered martensite strengthening; FM: fresh martensite strengthening; P: precipitation strengthening; SS: solid solution strengthening due to Cu and Ni; C: carbides.

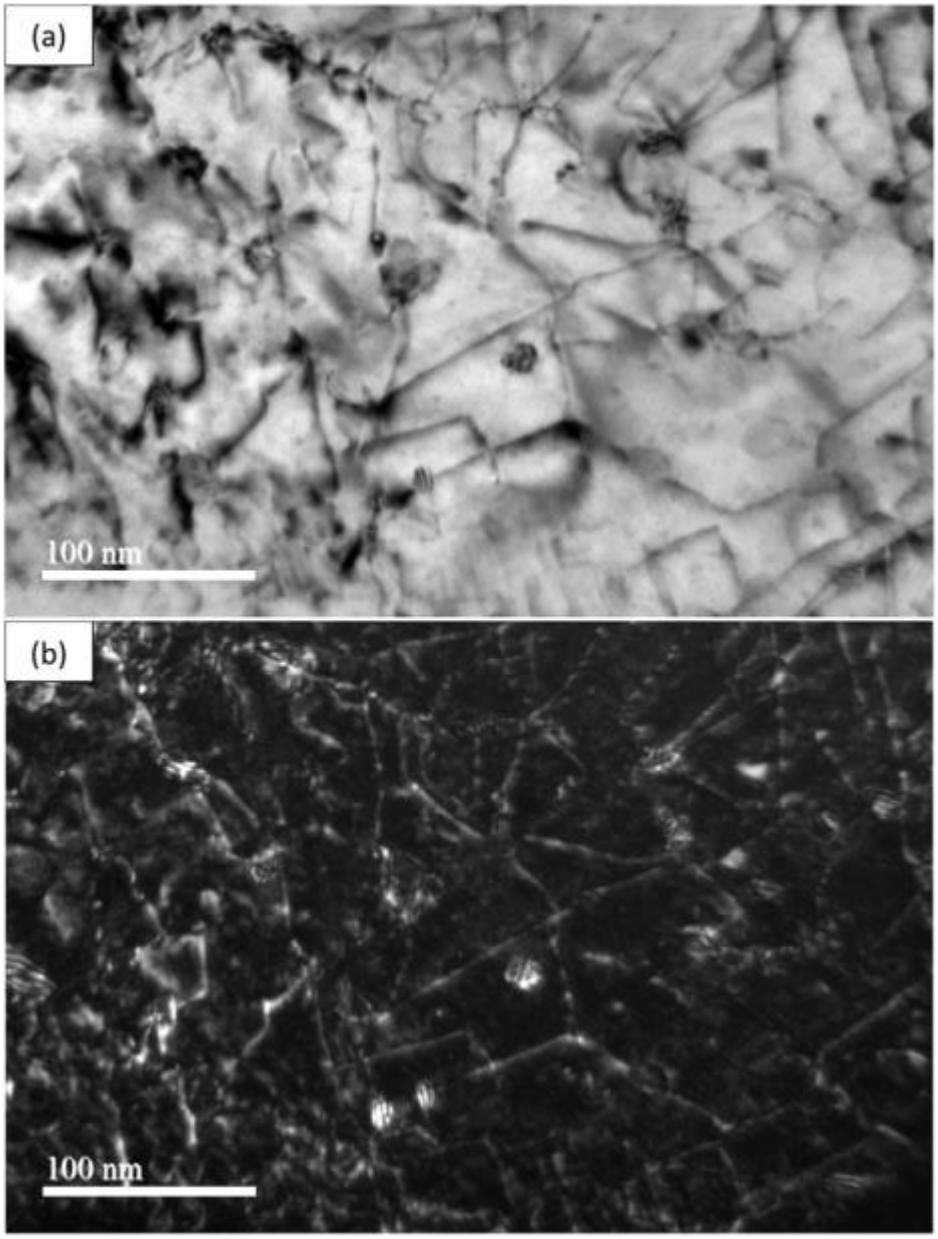

Fig. 10. TEM images showing dislocations cutting through overaged (~30 nm) Cu-rich precipitates of the fractured WQ/640C/10h/WQ tensile specimen in (a) bright field and (b) dark field.